

# Search for stripes in antiferromagnetic lightly hole-doped $\text{YBa}_2\text{Cu}_3\text{O}_6$ : An electron spin resonance and infrared transmission study

András Jánossy,<sup>1,\*</sup> Kálmán L. Nagy,<sup>1</sup> Titusz Fehér,<sup>1,2</sup> László Mihály,<sup>3</sup> and Andreas Erb<sup>4</sup>

<sup>1</sup>*Budapest University of Technology and Economics, Institute of Physics and Solids in Magnetic Fields Research Group of the Hungarian Academy of Sciences, P.O. Box 91, H-1521 Budapest, Hungary*

<sup>2</sup>*Institute of Physics of Complex Matter, EPFL, CH-1015 Lausanne, Switzerland*

<sup>3</sup>*Department of Physics and Astronomy, Stony Brook University, Stony Brook, New York 11794-3800, USA*

<sup>4</sup>*Walther Meissner Institut, Bayerische Akademie der Wissenschaften, D-85748 Garching, Germany*

(Received 25 May 2006; revised manuscript received 2 October 2006; published 2 January 2007)

We present a series of electron spin resonance (ESR) and infrared transmission experiments in antiferromagnetic (AF), lightly hole-doped  $\text{YBa}_2\text{Cu}_3\text{O}_6$  in search for the effect of a spatially inhomogeneous ground state on the magnetic and electric properties. Crystal compositions were  $\text{Ca}_x\text{Gd}_y\text{Y}_{1-x-y}\text{Ba}_2\text{Cu}_3\text{O}_6$  with  $x=0, 0.008, 0.02, \text{ and } 0.03$  and  $y \approx 0.01$ .  $\text{Gd}^{3+}$  ESR satellites from sites with first-neighbor Ca atoms show that holes are not preferentially localized at low temperatures in the vicinity of Ca dopants. We mapped by multifrequency  $\text{Gd}^{3+}$  ESR the AF domain structure as a function of hole concentration, temperature, and magnetic fields up to 8 T. We attribute the hole-doping-induced rotation of the magnetic easy axis from collateral to diagonal (with respect to the tetragonal  $\text{CuO}_2$  lattice) to the pinning of the AF magnetization to a static modulation or a phase-separated network of the hole density. The dominantly fourfold symmetry of pinning suggests that the hole density network has this symmetry also and is not an array of stripes. At higher temperatures the pinning to the diagonal direction becomes weak and the possibility of domain wall fluctuations is discussed. There is no magnetic field dependence and no in-plane anisotropy of the infrared transmission polarized in the  $\text{CuO}_2$  planes in an  $x=0.02$  crystal placed in magnetic fields up to 12 T. Thus, the network of holes is rigid and is not affected by magnetic fields that are, however, strong enough to rotate the AF magnetization into a single domain.

DOI: [10.1103/PhysRevB.75.024501](https://doi.org/10.1103/PhysRevB.75.024501)

PACS number(s): 74.72.Bk, 75.25.+z, 75.50.Ee, 76.30.Kg

## I. INTRODUCTION

### A. Electronic phase separation in hole-doped cuprates

The phase diagram of lightly hole-doped cuprates has a remarkable complexity. 3% holes/Cu introduced into the  $\text{CuO}_2$  planes of the two best studied cuprates,  $\text{La}_2\text{CuO}_4$  and  $\text{YBa}_2\text{Cu}_3\text{O}_6$ , destroys the long-range antiferromagnetic (AF) order of the Mott insulator parent compounds. A superconducting ground state is established at somewhat higher concentrations. There is growing experimental evidence for a spatial inhomogeneity in this transition region where early theoretical studies predicted an instability of the electronic structure. Mean-field calculations of the Hubbard model lead to a CDW and coupled SDW type of instability,<sup>1-4</sup> while calculations of the  $t$ - $J$  model suggest an electronic phase separation<sup>5</sup> (for a recent review, see Ref. 6). Although details are different, most studies suggest a one-dimensional (1D) modulation visualized by an array of charge-rich “stripes” separating charge-poor antiferromagnetic regions. The phase of the antiferromagnetic order changes by  $\pi$  across stripes. (Sometimes stripes are described as “domains” separated by  $180^\circ$  domain walls, but here we shall use the term “domains” to describe regions having nonparallel, usually orthogonal, sublattice magnetizations.) Other authors (Refs. 7 and 8 and references therein), however, predict a phase separation into a two-dimensional (2D) network of charge-rich regions. Recently, Horowitz discussed<sup>9</sup> the theoretical implications of some of the present electron spin resonance (ESR) results. Models with spiral AF modulation around single charged holes have also been developed<sup>6,10</sup> to explain dilute hole-doped systems.

The discovery of well-defined, stripelike spin-density and charge-density modulations in  $\text{La}_2\text{NiO}_{4+x}$ <sup>11</sup> motivated investigations of the possible electronic phase separation in the cuprates also. In hole-doped  $\text{La}_2\text{CuO}_4$  compounds a magnetic modulation has been observed in a range of doping extending from the lightly doped AF phase well into the superconducting phase. At low doping levels and low temperatures these fluctuations condense into a static modulated structure<sup>12</sup> with a wavelength inversely proportional to the hole doping.<sup>13,14</sup> In weakly hole-doped antiferromagnetic  $\text{La}_{2-\delta}\text{Sr}_\delta\text{CuO}_4$  (LaSCO) crystals the modulation runs along a diagonal of the underlying slightly distorted tetragonal  $\text{CuO}_2$  lattice, while in more doped superconducting LaSCO the modulation is collateral, i.e., along the Cu-O-Cu line.<sup>15,16</sup> There is evidence for a 1D<sup>17</sup> modulation in untwinned LaSCO. Hole-doped  $\text{YBa}_2\text{Cu}_3\text{O}_{6+\delta}$  (YBCO) has a smaller orthorhombic distortion of the structure than LaSCO and is therefore better suited to decide whether the modulation is quasi-1D or forms a 2D network in an ideal  $\text{CuO}_2$  lattice. The findings of a 1D modulation by Mook *et al.*<sup>18</sup> have been contested by the inelastic neutron study of Hinkov *et al.*,<sup>19</sup> who report a magnetic modulation corresponding to a 2D collateral stripe network in untwinned oxygen-doped YBCO crystals.

### B. Electric conductivity in lightly doped cuprates

Lightly doped cuprates have an insulating ground state but they become metallic rapidly with increasing temperature. The hole-doped  $\text{CuO}_2$  planes are quasi-2D conductors,

and the in-plane conductivity is much larger than the out-of-plane conductivity along the  $c$  direction. A stripelike structure with straight rivers of metallic regions or with a 1D charge-density modulation is expected to have an anisotropic in-plane conductivity. However, evidence for this is controversial.

The observed in-plane conductivity of YBCO in high magnetic fields<sup>20</sup> is slightly anisotropic: the conductivity along the field exceeds the conductivity perpendicular to the field by a fraction of a percent. Ando *et al.*<sup>20</sup> suggest that this small anisotropy is due to magnetically oriented stripes, while we pointed out<sup>21</sup> that it more likely reflects an orthorhombic lattice distortion from magnetostriction and is unrelated to stripes. A detailed analysis of the magnitude of the anisotropy supports the latter idea.<sup>22</sup> Undoped and lightly doped YBCO are not exactly tetragonal, as the AF sublattice magnetization in the  $\text{CuO}_2$  plane induces a slight orthorhombicity. The multidomain AF structure with orthogonal domains of the two possible distortions has been identified by neutron diffraction<sup>23</sup> and ESR.<sup>24</sup> Magnetic fields in the plane alter the AF domain structure and a sufficiently high magnetic field will result in a single AF domain with sublattice magnetization perpendicular to the field. The small conductivity anisotropy may result from the uniform distortion in the magnetically single crystal. The crucial dc experiment is yet to be done: while the conductivity anisotropy from magnetostriction is much smaller for a field along  $[110]$  than for fields along  $[100]$ , no such reduction is expected for stripes.

In untwinned LaSCO an in-plane magnetic-field-induced conductivity anisotropy has also been attributed to conducting stripes.<sup>25</sup> However, just like for YBCO, there is no clear evidence that this results from a stripe structure rather than from magnetostriction. Magnetostriction in LaSCO is likely to affect the conductivity, as magnetic fields induce ferrimagnetism and strong fields even change the crystal structure irreversibly.<sup>26</sup>

The absence of a large stripe-related anisotropy at zero frequency could be due to a pinning of the 1D charge-density modulation to defects. Pinning could shift the extra conductivity peak of stripes to finite frequencies, a phenomenon well known in quasi-1D conductors below the Peierls transition. Indeed, there are some indications for stripe-related electric excitations at infrared (IR) frequencies. Lightly hole-doped antiferromagnetic cuprates are insulating at low temperatures but the conductivity increases rapidly with frequency. Various low-frequency peaks in the conductivity have been assigned to conducting stripes.<sup>27,28</sup> An anomalous in-plane polarization-dependent Raman scattering peak in LaSCO at very low frequencies has been attributed to electric-field-driven excitations of stripes.<sup>28,29</sup> A similar Raman peak has been observed in the Ca-doped YBCO crystals<sup>30</sup> from the same batch as crystals discussed in this paper. The interpretation of the Raman spectra involves a diagonal stripe structure that is confirmed by the present study. The conductivity anisotropy at zero frequency and the IR and Raman spectroscopic observations inspired our search for a magnetic-field-induced anisotropy in the transmission of far IR radiation.

### C. Scope

We report in this paper on the antiferromagnetic domain structure of lightly hole-doped YBCO crystals. Section II describes the multifrequency  $\text{Gd}^{3+}$  ESR characterization of the AF structure. An in-plane magnetic anisotropy is found, which we attribute to the pinning to an underlying ordered hole structure. The electronic spin relaxation rate of the  $\text{Gd}^{3+}$  probe has an out-of-plane anisotropy attributed to the anisotropic magnetic polarization of mobile holes. To see whether magnetic fields affect the charge distribution, we search for an anisotropy in the conductivity in the IR transmission under magnetic fields that wipe out the domain structure. Section III details the IR transmission measurements, which prove to be negative: we find no conductivity anisotropy associated to stripes in a magnetically single crystal. The implications of the ESR and IR transmission results to the stripelike electronic phase separation are described in Sec. IV.

## II. ANTIFERROMAGNETIC DOMAIN STRUCTURE OF HOLE-DOPED YBCO

### A. Samples

Experiments were on  $\text{Ca}_x\text{Gd}_y\text{Y}_{1-x-y}\text{Cu}_2\text{Ba}_3\text{O}_6$  single crystals with  $x=0, 0.008, 0.02, 0.03$ , and  $y$  between 0.01 and 0.03. We denote samples from various batches as “Undoped”, “Ca0.8%”, “Ca2%”, and “Ca3%”. Crystals were grown in  $\text{BaZrO}_3$  crucibles as described elsewhere.<sup>31</sup> Oxygen reduction was obtained by a heat treatment in pure Ar atmosphere at a temperature of 700 °C. Typical sample dimensions are  $1 \times 1 \text{ mm}^2$  in the  $(a, b)$  plane and about 50  $\mu\text{m}$  along  $c$ . For all concentrations two or more crystals were tested by ESR with the same results. The Ca concentrations were determined by energy-dispersive x-ray analysis and are in approximate agreement with the ESR intensities of the first Ca neighbor  $\text{Gd}^{3+}$  satellites.<sup>32</sup> The nominal Gd concentration was 0.01 in all crystals. This agrees with estimates of the Gd concentration from the ESR dipolar satellites of  $\text{Gd}^{3+}$ - $\text{Gd}^{3+}$  pairs in three of the batches, while in Ca2% the Gd concentration measured from ESR is 3%. Some ESR experiments in Undoped and Ca0.8% samples were discussed in Ref. 32.

### B. Method to determine the antiferromagnetic domain structure

$\text{Gd}^{3+}$  has been extensively used as an ESR probe in high- $T_c$  cuprate superconductors and related antiferromagnets (see, e.g., Refs. 33–35). The  $J_{\text{Gd}}=7/2$  angular momentum interacts weakly with the  $\text{CuO}_2$  sandwich and probes local charge and spin distributions similarly to an NMR probe. As described in the Appendix, the resonance fields of the fine structure lines are shifted by the exchange interaction between the  $\text{Gd}^{3+}$  probe and the  $\text{CuO}_2$  magnetization. There are two contributions,

$$\Delta B_1 = -{}^{\text{Gd}}A\chi B \quad (1)$$

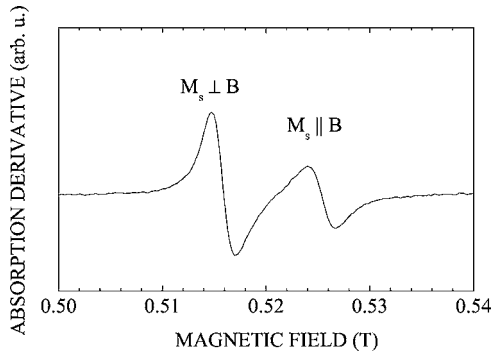


FIG. 1. Splitting of the highest field line in the  $\text{Gd}^{3+}$  ESR spectrum of the undoped YBCO single crystal at  $T=25$  K and  $f=9$  GHz with  $B\parallel[100]$  demonstrating the existence of collateral AF domains with easy axis parallel and perpendicular to the field. Domains with easy axis parallel to  $B$  have an angular distribution as they are affected by the field, and this decreases the amplitude of the  $M_s\parallel B$  line.

$$\Delta B_2 = C_m \chi. \quad (2)$$

The “ESR Knight shift,”  $-\Delta B_1/B$ , is independent of the external field,  $B$ , and is the same for all fine structure lines. It has been measured in both the antiferromagnetic and superconducting cuprates.<sup>36</sup> The “second order” shifts,  $\Delta B_2$ , are independent of the magnitude of  $B$  and are different for the various fine structure lines,  $m$ . Both shifts (1) and (2) are proportional to the macroscopic spin susceptibility,  $\chi$ , of the AF domain in which the  $\text{Gd}^{3+}$  probe is located. The constants  $G^d A$  and  $C_m$  are independent of doping and temperature. As explained in the Appendix, if the AF order is collateral then the second-order shifts are formally equivalent to shifts that would arise from magnetostriction, as we proposed for undoped YBCO in an earlier study.<sup>24</sup> However, for a consistent description of the data the second-order  $\text{Gd}^{3+}$  shifts must have a dominantly magnetic origin [as given by Eq. (2)] for both undoped and weakly hole-doped YBCO.

Since  $\chi$  and thus the resonance field depends on the angle between the sublattice magnetization,  $M_s$ , and the applied field,  $B$ , ESR spectra in the  $\text{CuO}_2$  planes allow the determination of the orientation of  $M_s$  or its angular distribution. Below we report on findings in the Undoped, Ca0.8% and Ca2% samples in magnetic fields between 0.2 T and 8 T in the [100] and [110] directions. In sample Ca3% we could not resolve an angular distribution of  $M_s$ ; either the linewidth is too large or the domains are no more static.

### C. Antiferromagnetic domain structure in low magnetic fields

The multidomain AF structure is evident in the Undoped, Ca0.8% and Ca2% samples at low magnetic fields and low temperatures. Figure 1 shows the highest field fine structure line corresponding approximately to the  $7/2 \rightarrow 5/2$  transition at 9 GHz. The line is split into a broader, smaller amplitude line and a narrower, stronger line corresponding to  $M_s\parallel B$  and  $M_s\perp B$  domains, respectively. The maximum separation between the split lines is the same for all three samples, but it occurs at  $B\parallel[100]$  for the undoped and at  $B\parallel[110]$  for the

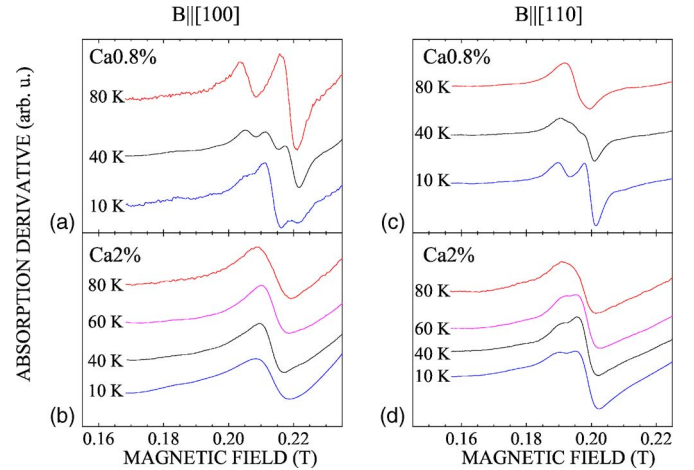


FIG. 2. (Color online) The lowest field fine structure line at 9 GHz showing variation of the AF easy axis with doping and temperature. Panels a and c: In sample Ca0.8% the easy axis gradually changes from low-temperature diagonal to high-temperature collateral. At 40 K both collateral and diagonal phases appear and three lines are observed: (i) domains aligned  $M_s\perp B$ , (ii)  $M_s$  inclined by  $\pi/4$  from  $B$ , and (iii)  $M_s\parallel B$ . These have  $\chi$ ,  $\chi/2$  and zero susceptibilities, respectively, and show maximum, intermediate, and zero shifts to higher fields. (We note that the “ESR Knight shift” has no observable contribution at these fields.) At 10 K most of the domains are diagonal. For  $B\parallel[100]$  (panel a) most of the line corresponds to  $\chi/2$  susceptibility. For  $B\parallel[110]$  (panel c) two lines corresponding to  $\chi$  and zero susceptibilities appear. At 80 K the easy axis is collateral and the  $B\parallel[100]$  is split while the  $B\parallel[110]$  line is unsplit. Panels b and d: The Ca2% sample has a diagonal easy axis at 10 K which persists up to at least 60 K. At 80 K AF domains are either fluctuating or transformed into a single perpendicular domain by the field.

doped samples. The line is unsplit for  $B\parallel[110]$  for the undoped and at  $B\parallel[100]$  for the doped samples, as shown in Fig. 2. This corresponds to a collateral AF easy axis in the undoped sample and a diagonal easy axis in the two hole-doped crystals at low temperatures. The fine structure parameters were determined from a fit to the spectra. The principal axes are rotated by  $\pi/4$  between the undoped and doped samples, but the magnitude of  $b_2^2$  is the same,  $b_2^2=48$  MHz. Since  $b_2^2$  is proportional to the magnetic susceptibility [see Eq. (A5b)], this means that the principal axes of  $\chi$  rotate by  $\pi/4$ , but the *magnitude* of  $\chi$  is independent of doping concentration.

In the undoped sample the collateral AF domain structure is independent of temperature. On the other hand, the hole-doped samples have a temperature-dependent AF structure (Fig. 2). In the Ca0.8% doped samples a gradual transition is observed from mostly diagonal at low temperatures to mostly collateral above 40 K. The collateral multidomain structure is observed up to 200 K. In the Ca2% sample the easy axis is diagonal from low  $T$  to at least 60 K. At higher temperatures a single line is observed for both  $B\parallel[100]$  and  $B\parallel[110]$ ; thus, the AF structure is single domain or there are domains fluctuating between two orthogonal directions. The easy axes at various temperatures and hole doping are summarized in a phase diagram in Fig. 3.

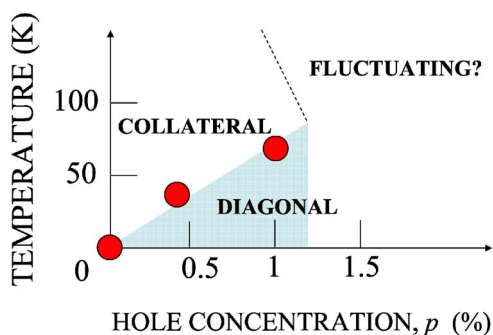


FIG. 3. (Color online) Temperature vs hole concentration phase diagram of the antiferromagnetic easy axis in lightly doped YBCO measured by ESR. The dashed line indicates the separation between an observed static AF structure with a well-defined anisotropy and an AF structure with fluctuating orthogonal domain walls and/or a very small anisotropy. The data point at  $p=0.4\%$  (sample Ca0.8%) corresponds to the temperature where roughly equal amounts of collateral and diagonal phases were observed. The data point at  $p=1\%$  (sample Ca2%) corresponds to the temperature where the diagonal domain structure is no more resolved in the ESR spectra.

#### D. Antiferromagnetic domain structure in high magnetic fields

In zero field the antiferromagnetic sublattice magnetization,  $M_s$ , of AF domains is oriented equally along the two possible easy directions. A sufficiently large field,  $B$ , oriented arbitrarily in the  $\text{CuO}_2$  plane rotates the domains into the  $M_s \perp B$  direction. The rearrangement of domain orientations is reversible: the ESR spectra do not depend on magnetic field or temperature history. The field required to align most domains into a magnetically single crystal is a measure of the pinning strength of the magnetization to the lattice. It has a nontrivial anisotropy in the  $\text{CuO}_2$  plane that reflects the symmetry of the pinning structure. We find that it is *easier* (i.e., a smaller field is required) to rotate a typical domain perpendicular to a magnetic field oriented along its easy direction and *harder* along an angle inclined by  $\pi/4$  from the easy direction. We denote by  $B_{ce}$  (“ $B$  critical easy”) and  $B_{ch}$  (“ $B$  critical hard”) the characteristic fields along the magnetic easy axis and inclined by  $\pi/4$ , respectively, as shown in Fig. 4. The detailed measurements (summarized for Ca2% in Table I) show that  $B_{ch} > B_{ce}$  for the Undoped, Ca0.8% and Ca2% crystals at low temperatures. As explained in Sec. IV C,  $B_{ce}$  characterizes a twofold symmetric magnetic anisotropy arising from, e.g., linear stripes.  $B_{ch}$  is characteristic of a fourfold anisotropy that can arise from magnetostriction or a tetragonal arrangement of stripes.

Results for the characteristic fields in the present undoped crystals grown at the Walther Meissner Institut (WMI) and the undoped crystals grown at the University of Oxford reported in Ref. 24 are similar. In the Ca0.8% sample the high field spectra at intermediate temperatures are complicated by the interplay of the change of the easy axis with temperature and the rotation of  $M_s$  by the magnetic field. Fields above 1 T change the spectra (i.e., rearrange the domains) significantly at all temperatures.

Table I summarizes the effect of a magnetic field on the orientation of domains (i.e., of  $M_s$ ) in the Ca2% crystal. At 20 K a magnetic field of 0.2 T has little effect on the AF

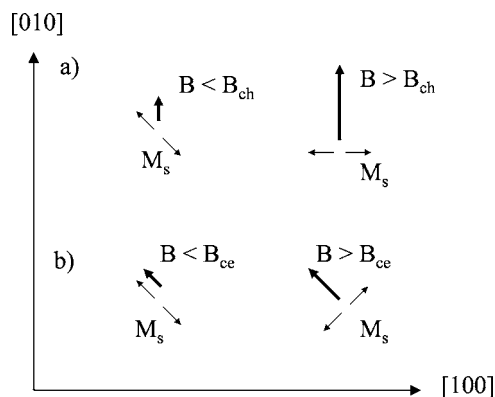


FIG. 4. The anisotropy of the magnetic field required to rotate most of the AF domains perpendicular to the field. Experiments show that for the lightly doped Ca0.8% and Ca2% samples, a smaller field,  $B_{ce}$ , is required along the  $[110]$  AF easy axis than  $B_{ch}$  along the  $[010]$  AF hard axis, i.e.,  $B_{ce} < B_{ch}$ .

structure: the sample consists of both types of domains. A field of 2.7 T along the tetragonal  $[110]$  direction rotates most of the domains that have an easy axis along the field, and the sample is almost a magnetic single domain with  $M_s$  along the  $[\bar{1}10]$  direction. (In the 75 GHz  $B \parallel [110]$  spectra a weak shoulder is observed at low temperatures, corresponding to a small amount of  $M_s \parallel B$  domains left intact by the field.) The characteristic field at 20 K along the easy axis is thus  $B_{ce} \approx 2.7$  T. On the other hand, as explained below, a field of 2.7 T along the  $[100]$  hard axis is insufficient to rotate the magnetization significantly; thus, the characteristic field along the hard axis is  $B_{ch} > 2.7$  T.

For  $B \parallel [100]$  the angle of  $B$  is the same with respect to both types of domains and a single fine structure series is observed. In this case the orientation distribution of  $M_s$  has to be determined from the susceptibility. Figure 5 shows the susceptibility obtained from a fit to the observed spectra using Eqs. (A1), (A2), and (A4) and the temperature-dependent fine structure parameters listed in Ref. 24. The precise orientation of the crystal was also derived from the ESR spectra. As seen in Fig. 5, for  $B \parallel [100]$   $\chi$  increases by a factor of 2 when the temperature is raised above 40 K, as expected if  $M_s$  rotates by  $\pi/4$  from diagonal to collateral. Results at 20 K are unambiguous: the crystal has a diagonal multidomain structure at a field of 2.7 T, while it is a single magnetic domain at 8 T field applied in any direction of the  $\text{CuO}_2$  plane. Thus,  $B_{ce}$  is less than  $B_{ch}$  at 20 K, and we find  $B_{ce} \approx 2.7$  T and  $8 \text{ T} > B_{ch} > 2.7$  T.

As shown in Table I, at high temperatures domains are rotated perpendicular to fields equal or larger than 2.7 T and applied along the  $[100]$  direction. In other cases the AF structure could not be unambiguously determined. No splitting of the fine structure has been observed at low fields in spite of the relatively narrow lines. This may signify a rapid fluctuation of domains between the two diagonal easy axes or a static domain structure with a weak anisotropy that allows the domains to rotate perpendicular to low fields. Unfortunately, experimental uncertainties were too high to determine the susceptibility from the spectra at low fields and high temperatures and we cannot decide between the two possi-

TABLE I. Variation of the AF structure with external field at low and high temperatures in the Ca2% sample. At 100 K and low fields the possibilities of fluctuating orthogonal domain walls or static domains rotated perpendicular to small fields (i.e., small anisotropy) could not be distinguished by ESR. Under the conditions of the IR transmission experiment, i.e., at low temperature and high fields, the sample is magnetically a single domain.

Field orientation	Field	AF domain orientation 20 K	AF domain orientation 100 K
[110]	0.2 T	Diagonal Multidomain	Diagonal single domain? Fluctuating?
[110]	2.7 T	Diagonal, Mostly $M_s \perp B$	Single domain? Fluctuating?
[110]	8.1 T	Diagonal Single domain	Single domain? Fluctuating?
[100]	0.2 T	Diagonal Multidomain	Diagonal multidomain? Fluctuating?
[100]	2.7 T	Diagonal Multidomain	Collateral Single domain
[100]	8.1 T	Collateral Single domain	Collateral Single domain

bilities. A weaker anisotropy will increase the fluctuations in any case; thus it is probable that at some high temperatures  $\pi/2$  domain walls fluctuate.

#### E. Perturbation of charge distribution near the Ca sites

Holes introduced to the  $\text{CuO}_2$  sheets in concentrations below 3-4% hole/Cu are known to localize at low temperatures.<sup>12</sup> The question arises whether the holes are localized near the  $\text{Ca}^{2+}$  ions from where they are issued or else in phase-separated regions?

The zero field splitting is modified for  $\text{Gd}^{3+}$  with first-neighbor Ca ions, and a series of satellite lines is observed near the main ESR transitions.<sup>32</sup> The intensity of satellites

increases with Ca concentration, justifying our assignment of lines (Fig. 6). As a further test, we measured Ca0.8% in tilted fields to show that Ca satellites are first and not second neighbors. All satellite  $\text{Gd}^{3+}$  sites are equivalent in a magnetic field along the [001] (i.e.,  $c$ ) direction but there are two

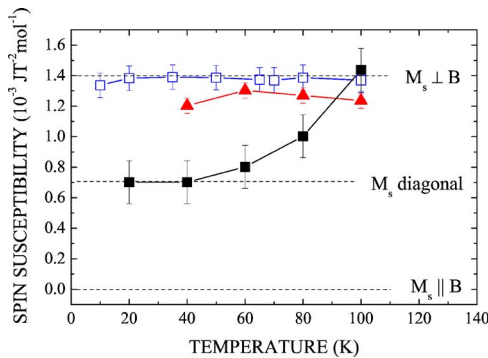


FIG. 5. (Color online) Spin susceptibility,  $\chi$ , of the  $\text{CuO}_2$  layers vs temperature for  $B \parallel [100]$  derived from the  $\text{Gd}^{3+}$  ESR shift. Open squares: Undoped at 2.7 T, full squares: Ca2% at 2.7 T, and full triangles: Ca2% at 8.1 T. At low temperatures the AF easy axis is diagonal and a relatively large magnetic field,  $B > 2.7$  T, is required to rotate the sublattice magnetization,  $M_s$ , perpendicular to the field. As shown by the increase of  $\chi$ , at higher temperatures pinning to the lattice is weaker, e.g., at 100 K  $M_s$  rotates perpendicular to  $B$  at 2.7 T.

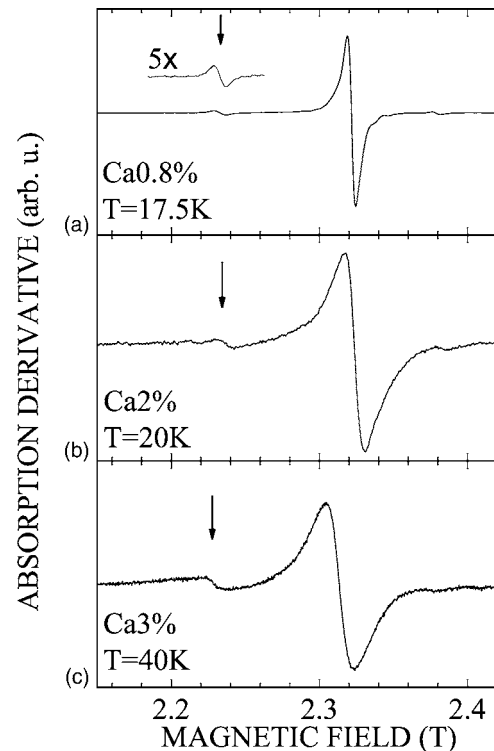


FIG. 6. The  $7/2-5/2$   $\text{Gd}^{3+}$  ESR transition at 75 GHz for  $B \parallel c$  in samples (a) Ca0.8%, (b) Ca2%, and (c) Ca3%. The arrows mark the Ca satellites, i.e., the signal from  $\text{Gd}^{3+}$  ions that have a first-neighbor Ca, while the main line corresponds to  $\text{Gd}^{3+}$  without Ca first neighbors.

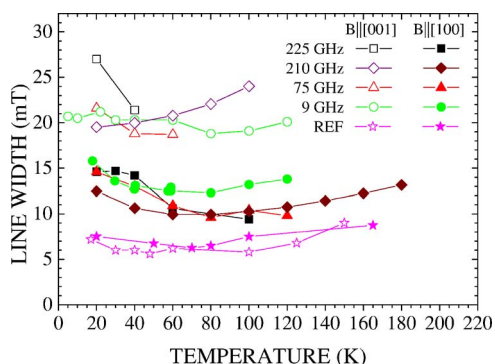


FIG. 7. (Color online) Peak-to-peak linewidths of the  $7/2 \rightarrow 5/2$   $Gd^{3+}$  ESR transition vs temperature at several frequencies in sample Ca3%. REF is the linewidth of the Undoped sample at 75 GHz. We omitted high-field data below 20 K where the lines are broadened by  $Gd^{3+}$ - $Gd^{3+}$  dipolar interactions.

inequivalent sites in tilted fields. We observed a splitting of the satellite line for fields tilted within the  $(a, c)$  plane, as expected for first neighbors. For second neighbors the line would split for  $B$  in the  $(c, [110])$  plane.

The observation of an essentially temperature-independent  $Gd^{3+}$  ESR at sites near Ca atoms confirms that holes are not localized at low temperatures to the  $Ca^{2+}$  ions for the following reasons. The Ca satellite shift is due to the change of the fine structure when one of the four  $Y^{3+}$  neighbors of a  $Gd^{3+}$  probe is replaced by  $Ca^{2+}$ . The fine structure is very sensitive to changes of the charge distribution. If holes were localized at low temperatures preferentially in the vicinity of Ca ions, then temperature-dependent shifts several times the linewidth would occur. For example, the largest fine structure parameter,  $b_2^0$ , increases gradually with oxygen doping,  $\delta$ , in  $YBa_2Cu_3O_{6+\delta}$ <sup>35</sup> and is 50% larger in  $YBa_2Cu_3O_7$  than in  $YBa_2Cu_3O_6$ , i.e., when hole concentration changes from zero to  $\sim 0.16$  holes/Cu. This hole doping shifts the  $7/2$ - $5/2$  transition in  $YBa_2Cu_3O_7$  by about 40 times the linewidth in Ca0.8%. Thus, a small fraction of a hole localized preferentially on the first-neighbor atoms of Ca dopant would be detected. Observations on the Ca2% and Ca3% samples confirm the results of Ref. 32 obtained for the Ca0.8% sample: no temperature-dependent change of shift with respect to the main lines was observed.

#### F. Anisotropy of ESR linewidths

The fine structure components of the Ca0.8% and Undoped samples have isotropic ESR linewidths. At low temperatures the linewidth is about 60 G, which gradually increases above 100 K. In contrast, the more doped samples, Ca2% and Ca3%, have an increased linewidth with large anisotropy in the  $(a, c)$  plane (Fig. 7). There is no significant anisotropy within the  $CuO_2$  plane.

### III. SEARCH FOR AN IN-PLANE IR CONDUCTIVITY ANISOTROPY

The aim of these experiments was to find an anisotropy in the infrared conductivity in the frequency range of

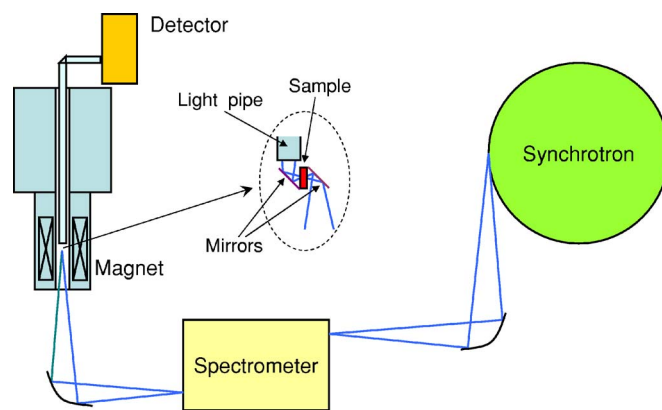


FIG. 8. (Color online) Spectrometer for IR conductivity measurements under magnetic field. The enlargement sketches the sample holder for magnetic field parallel to the surface of the plate-like sample. Polarization of IR radiation incident on the sample surface is changed by rotating the sample together with mirrors and a light pipe around the vertical axis.

10–90  $cm^{-1}$  that could arise from a stripelike electronic phase separation or modulation. We compare the transmission through the Ca2% sample in a high magnetic field to transmission in zero field. The sample is macroscopically isotropic in zero field while it is a magnetically anisotropic single crystal when a high enough field is applied in the  $(a, b)$  plane. Various combinations of magnetic field orientations and IR polarization were tested at temperatures between 4 and 126 K.

The experimental setup at the U12IR beamline of the Brookhaven National Synchrotron Light Source facilities is shown in Fig. 8. A detailed description of the apparatus is given in Ref. 37. In the special probe head built for the present experiments, the vertical static magnetic field,  $B$ , is in the  $(a, b)$  plane of the sample: experiments are performed with  $B$  along the  $[100]$  and  $[110]$  axes. Light is transmitted horizontally along the  $[001]$  or  $c$  axis of the sample. The polarization of the infrared electric field in the  $(a, b)$  plane can be set parallel or perpendicular to the static magnetic field by rotating the polarization of the incoming light. The various combinations of static and IR fields and crystal orientations are shown in Fig. 9. Figure 10(a) shows the raw transmission data through (i) the roughly 1 mm diameter hole of the probe head, (ii) the Undoped sample, and (iii) the Ca2% sample covering the same hole. The frequency dependence of the transmission through the hole with no sample results partly from the characteristics of the source and partly from limitations imposed by the probe head. The beam splitter used in the spectrometer decreases substantially the intensity at 25, 50, and 75  $cm^{-1}$ . The absorption in the undoped sample is relatively small, and transmission oscillations due to multiple reflections between sample surfaces are still clearly observed [Fig. 10(b)]. The transmission is strongly reduced in the Ca2% doped sample. We detected the  $Gd^{3+}$  ESR in the Ca2% sample at 11 and 12 T when spectral resolution was increased to 0.5  $cm^{-1}$ , and this confirms that the transmission is indeed through the sample and not a leakage around the sample. Transmission through the Ca3% sample was too weak to be measured.

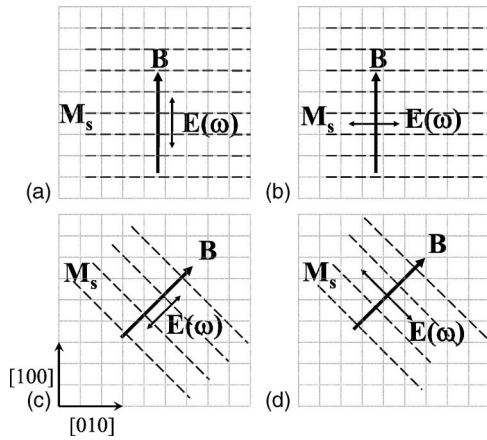


FIG. 9. Geometrical arrangements of the infrared (IR) transmission experiments.  $B$ : static magnetic field;  $M_s$ : sublattice magnetization;  $E(\omega)$ : polarization of the IR electric field. IR propagation is along  $[001]$ . (a) and (b)  $B$  along the  $[100]$  crystallographic axis of the YBCO crystal; (c) and (d)  $B$  along the  $[110]$  axis.

Figures 10(b) and 10(c) show the transmission through the undoped and Ca2% samples at 4 K with  $B=0$  and 12 T using the geometries of Figs. 9(a) and 9(b), respectively. Data for geometries shown in Figs. 9(c) and 9(d) are of similar quality. Differences between transmission with and with-

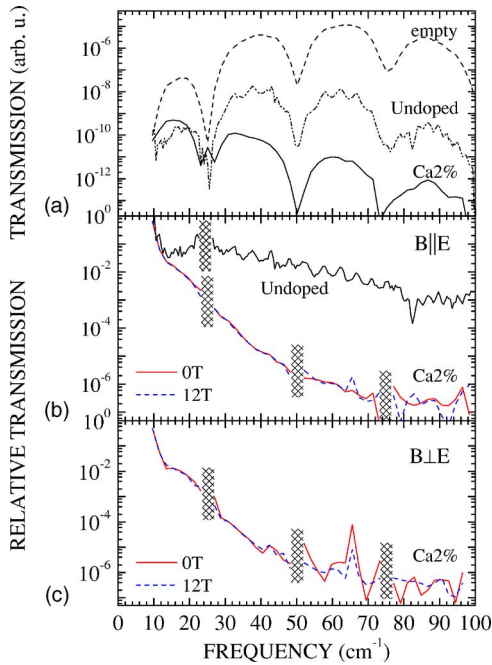


FIG. 10. (Color online) IR transmission through the Ca2% single crystal. No dependence is found on magnetic field or polarization. (a) Raw transmission data through the empty sample holder, the undoped single crystal, and the Ca2% single crystal. (b) and (c) compare transmissions in zero field (continuous lines) and 12 T field (dashed lines) normalized to transmission through the empty sample holder. Incident light is weak at 25, 50, and 75  $\text{cm}^{-1}$ , and corresponding transmission data are omitted for clarity. (b) Undoped and Ca2% in the geometry of Fig. 9(a), and (c) Ca2% in the geometry of Fig. 9(b).

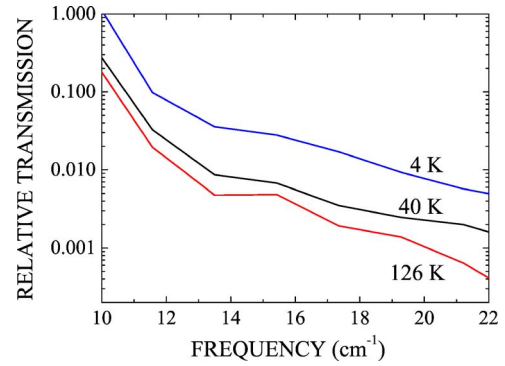


FIG. 11. (Color online) The temperature dependence of the transmission through sample Ca2% normalized to the transmission through the empty sample holder.

out magnetic field are within experimental uncertainty, and we estimate that the magnetic field changes the transmission by less than  $\pm 5\%$  in the full spectral range. The field-induced anisotropy in conductivity with respect to the isotropic conductivity,  $\sigma$ , is much less than this since the sample is thicker than the penetration depth,  $\delta = (\omega\mu_0\sigma/2)^{-1/2}$ , and the transmission is proportional to  $\exp(-l/\delta)$ , where  $l$  is the thickness of the sample.

The conductivity in the 10  $\text{cm}^{-1}$  to 90  $\text{cm}^{-1}$  IR range is high compared to the zero frequency conductivity, especially at low temperatures. The decrease of transmission with increasing temperature is moderate (Fig. 11). The factor of six change in transmission at 15  $\text{cm}^{-1}$  between 4 and 126 K corresponds to a rather small change in conductivity, since the penetration depth is shorter than the sample thickness. For comparison, the dc (zero frequency) in-plane conductivity in a 3% Ca sample was immeasurably small at 4 K, and it increased rapidly with temperature and changed by two orders of magnitude from 20 K to 125 K. Although we have not measured the in-plane dc conductivity in the Ca2% sample, it certainly has a similar transition from an insulating to a metallic behavior.

## IV. DISCUSSION

### A. Observations supporting an ordered structure of holes

Here we list observations supporting the idea that stripes or other forms of phase-separated regions (“stripe networks”) are formed in YBCO at small hole doping concentrations.

It is well known from resistivity and muon spin rotation<sup>12</sup> experiments that holes are delocalized at high temperatures and are localized at low temperatures, typically below 20 K in the low-doped antiferromagnetic phase. From the temperature independence of the shift of first-neighbor Ca satellites of the  $\text{Gd}^{3+}$  ESR, we concluded (Sec. II E) that at low temperatures holes are not localized to the randomly distributed Ca ions from which they originate. This supports the idea of an ordered structure of holes independent of Ca distribution. There are no other obvious sites for localization of single holes than the Coulomb potential of the excess charge at  $\text{Ca}^{2+}$  ions.

A small concentration of holes changes the easy axis of the AF sublattice magnetization,  $M_s$ , from collateral to diag-

onal without changing the magnitude of the susceptibility. At the lowest hole concentration,  $x=0.008$  ( $p=0.4\%$  /Cu), the low-temperature diagonal easy axis changes gradually to collateral in a broad temperature range of 10–80 K. The diagonal easy axis is more stable in the Ca2% sample, which has a diagonal easy axis up to at least 60 K. It is unlikely that randomly localized holes in such a small concentration could change the easy axis of  $M_s$ . On the other hand, an ordered network of phase-segregated holes may determine the low-temperature easy axis of the bulk without changing the susceptibility, which is determined by the Cu-O-Cu exchange,  $J$ , of the hole-poor bulk. The larger stability of the diagonal spin modulation at higher hole concentration (Fig. 3) supports this idea also.

### B. Absence of magnetic field-induced IR conductivity anisotropy

The most likely reason for no appreciable conductivity anisotropy in the lightly hole-doped (magnetically) single crystal is that the network of charge modulation is rigid at the energy scale of interactions with a magnetic field of 12 T. The magnetic fields that rearrange the AF structure leave the underlying network of holes unchanged. The much stronger long-range Coulomb interactions easily stabilize the network.

As explained above, in our view the small zero-frequency conductivity anisotropy is due to magnetostriction. It is unlikely that the conductivity anisotropy is negligible at low frequencies only and becomes large at higher frequencies, well above our detection limit of  $90\text{ cm}^{-1}$ . For this the charge associated with stripes should be very strongly pinned to the lattice. However, it would be difficult to explain the large hole-induced low-temperature isotropic conductivity at frequencies above  $10\text{ cm}^{-1}$  if holes were strongly pinned. It is much more likely that holes are weakly pinned to the lattice at low temperature and are excited above a pinning frequency in the range of 10–100  $\text{cm}^{-1}$ .

### C. Magnetic in-plane anisotropy and geometry of stripe network

We argue that the charge inhomogeneity of phase-separated hole-rich regions pin the AF magnetization to the lattice. We suggest that the network formed by holes is not an array of straight, parallel-running lines (“stripes”) but rather it has a two-dimensional pattern, e.g., like the egg-box pattern envisaged by Seibold *et al.*<sup>7</sup> Pinning is weak and is insufficient to stabilize a static magnetic structure at moderately high hole concentrations and temperatures.

We outline a simple phenomenological model to account for the essential observations of the static AF structure. The in-plane isotropic exchange interaction is very strong,  $J=1400\text{ K}$ ; therefore, we assume that the sublattice magnetization,  $M_s$ , in the  $i$ th  $\text{CuO}_2$  plane is uniformly oriented along  $\phi_i$ . The observed domains with orthogonal  $M_s$  are not in contradiction with this model: they may still exist either along  $c^{24}$  or in the  $(a,b)$  plane on a length scale larger than that of the stripes. We measure all angles from a Cu-O-Cu

direction fixed to the sample. The energy of the spin system is

$$E_i = -K_2 \cos 2(\phi_i - \phi_{0i}) - K_4 \cos 4(\phi_i - \phi_{0i}) - B^2 \chi/2 \cos^2(\phi_i - \phi_B) + A_i(i+1, i-1), \quad (3)$$

where  $\phi_B$  is the direction of the field,  $B$ , applied in the plane. The (positive) twofold and fourfold anisotropy energies  $K_2$  and  $K_4$  describe the coupling of  $M_s$  to the lattice.  $\phi_{0i}$  is the angle of the easy axis, i.e., the equilibrium orientation of  $M_s$  in the absence of  $B$ . The interbilayer interaction, denoted by  $A_i(i+1, i-1)$ , arises from weak exchange and dipolar interactions. We have to specify the boundary conditions at layers  $i=1$  and  $i=N$  bordering the crystal to define the complete problem. The pinning described by  $K_2$  and  $K_4$  can arise from the stripe network, magnetostriction, and defects in the crystal. If the easy axis is collateral, then  $\phi_{0i}$  can be  $\phi_{0i}=0$  or  $\phi_{0i}=\pi/2$ . In the diagonal case,  $\phi_{0i}$  is either  $\pi/4$  or  $3/4\pi$ . The pinning to a stripe network depends on its geometry: an array of parallel stripes contributes mainly to  $K_2$ , while a squarelike pattern or other two-dimensional patterns with equal amounts of orthogonal stripes within the plane yields  $K_4$  as the first nonzero term.

The simplest assumption is that pinning of  $M_s$  to the stripe network within the plane is more important than the coupling to the neighboring planes. A numerical analysis of the equilibrium determined by Eq. (3) when  $A_i(i+1, i-1)$  is neglected shows a fourfold anisotropy,  $K_4$ , comparable to or larger than the twofold anisotropy,  $K_2$ , if  $B_{ch}$  is larger than  $B_{ce}$ . Consequently, the stripe network introduces a nonnegligible fourfold symmetric anisotropy.

This conclusion remains valid if we consider the coupling to neighboring planes. As a second limiting case, we assume  $K_2=0$  and a finite  $A_i(i+1, i-1)$ . The role of twofold pinning anisotropy is taken over by a pinning at the borders of the stack of  $N$  planes. At the borders there is a strong pinning along one of the  $\phi_0$  easy directions. In a sufficiently high magnetic field,  $M_s$  is aligned perpendicular to the field at the center of the stack. The spins at the borders are aligned approximately along the pinning direction. The condition  $B_{ch} > B_{ce}$  is fulfilled if  $K_4$  is sufficiently large, but the details depend on the length of the chain and the interplane coupling.

Thus, the observations are described by a large in-plane fourfold anisotropy and a smaller twofold anisotropy. This is inconsistent with parallel running stripes for which, whatever the detailed mechanism of pinning  $M_s$ , the twofold anisotropy would be dominant. The observed fourfold anisotropy is compatible with pinning to a lattice of squarelike charged structure.

Magnetostriction could also contribute to  $K_4$  but this would be different for diagonal and collateral easy axes. In the collateral case magnetostriction changes the distance between the antiferromagnetic pairs as order sets in. On the other hand, if the order is diagonal then the distance between first-neighbor AF pairs is unchanged; only the distance between second neighbors, e.g., the angle between AF pairs changes. Intuitively a stronger effect is expected in the collateral case than the diagonal one. However, this is not ob-

served in the Ca0.8% sample where pinning is not much different in the high temperature collateral and the low temperature diagonal phases. Thus, it is likely that magnetostriction is of little importance in determining the pinning of the AF magnetization.

#### D. Diagonal-collateral phase diagram

Here we discuss the phase diagram of Fig. 3 deduced from experiment. Pinning of the magnetization in the collateral phase may arise from magnetostriction or from a stripe network with appropriate symmetry. The mechanism of pinning might be similar in the collateral phases of the Undoped and Ca0.8% samples, as we cannot rule out a low-concentration hole doping from some residual, uncontrolled defects, e.g., oxygen chain fragments in the Cu(1) planes. On the other hand, in the doped samples at low temperatures the pinning is entirely due to the stripe network. The Hubbard model calculation<sup>38</sup> of the geometry of stripes in the two-dimensional lattice suggests that the stripe network may change with temperature from diagonal to collateral. Indeed, the rotation of the easy axis of  $M_s$  may reflect the rotation of the stripe network. Alternatively, the change of the easy axis may reflect the disappearance of the rigid stripe network with temperature. In this interpretation, in the Ca0.8% sample the high-temperature collateral easy axis is due to some sample imperfections, which is overcome by the diagonal pinning at low temperatures. The data at higher doping concentrations suggest the fluctuation of the stripe network as the anisotropy disappears. The diagonal fourfold anisotropy disappears in the Ca2% sample above 80 K and is not replaced by a collateral anisotropy of similar magnitude. The anisotropic Gd<sup>3+</sup> ESR linewidths of samples Ca2% and Ca3% also indicate a fluctuation of the magnetic order in the CuO<sub>2</sub> plane, as explained below.

#### E. Domain wall fluctuations

Gd<sup>3+</sup> ESR is insensitive to fluctuations of largely spaced broad stripes ( $\pi$  domain walls), as the structure factor at the AF wave vector is zero at the highly symmetric rare earth position. Here we consider large amplitude fluctuations of the *orthogonal* domain walls (i.e., walls separating AF domains with orthogonal sublattice magnetizations) that are sensed by the Gd<sup>3+</sup> probes via the fluctuating spin susceptibility. Unfortunately, we have no information on the size and shape of orthogonal domains. Only if the fluctuations between the two orthogonal domains are slow on the time scale of the line separation,  $\Delta f = 3 \times 10^8$  Hz, is the splitting of the fine structure series observed. A single, motionally averaged fine structure series appears if fluctuations throughout the sample are faster than  $\Delta f$ .

In the Undoped and Ca0.8% samples the splitting of Fig. 1 is well resolved at all temperatures; therefore, orthogonal domain wall fluctuations must be weak. On the other hand, in the Ca2% sample the splitting gets less pronounced above 40 K and no splitting is observed in the  $B \parallel [100]$  or in the  $B \parallel [110]$  geometry at 80 K and higher temperatures (Fig. 2). Spectral resolution would be sufficient to resolve a splitting; the single line at 80 K is not much broader than the split

lines at 40 K. Thus, it is likely that the magnetocrystalline anisotropy at 80 K and above is overcome by thermal fluctuations of the domain structure. We cannot rule out, however, that in zero external field there is a static domain structure which is wiped out above 80 K by an external field as small as 0.2 T. In any case, the lack of a multidomain structure above 80 K signals a very small pinning to the lattice.

A single fine structure series is observed in the Ca3% sample at all magnetic fields and temperatures. We searched in vain for an unresolved splitting in the CuO<sub>2</sub> plane anisotropy of the linewidth in the 9 GHz spectra at several temperatures. Thus, orthogonal domain wall fluctuations may be strong. However, the linewidth is equal to the expected splitting, and this may hide a static distribution of domains.

#### F. Single carrier fluctuations

We attribute the increase of Gd<sup>3+</sup> ESR linewidth observed in the higher doping concentration samples, Ca2% and Ca3%, to single carrier spin fluctuations. Orthogonal domain wall fluctuations are unlikely to play a role, as no clear change is observed when domain walls are wiped out at high fields. The lines are probably not broadened inhomogeneously, as they are nearly perfect Lorentzians for  $T > 40$  K. In the Ca3% sample the anisotropy of the linewidth corrected for the isotropic linewidth of the undoped sample is about a factor of 2 (Fig. 7). This suggests that the linewidth anisotropy arises from a spin lifetime broadening by fluctuating fields oriented randomly in the CuO<sub>2</sub> plane but with no component perpendicular to the CuO<sub>2</sub> plane. The exchange field at the Gd sites of single hole excitations in the AF lattice have this character. Since only magnetic fluctuations perpendicular to the external field are effective in reducing the spin lifetime, single hole excitations are twice as effective for applied fields along  $c$  as in the CuO<sub>2</sub> plane. However, a detailed explanation of the effect is still missing.

### V. CONCLUSIONS

Gd<sup>3+</sup> ESR is a sensitive probe of the magnetic structure of YBCO. We mapped the phase diagram of the antiferromagnetic structure as a function of temperature in the lightly doped regime. A doping concentration below 1% is sufficient to stabilize a static diagonal AF structure at low temperatures instead of the collateral structure of undoped samples. In the Ca0.8% sample a transformation from diagonal to static collateral is observed with increasing  $T$ . Diagonal order was also observed in the Ca2% sample at low  $T$ , but no AF domains were resolved at high temperatures. In the Ca3% sample no AF domains were detected at any temperature. Large amplitude fluctuations of the domain walls between orthogonal AF domains is a likely reason for this, and the time scale of the experiment is  $10^{-8}$  s. In the Ca2% and Ca3% samples, an extra Gd<sup>3+</sup> spin relaxation appears which is attributed to mobile carriers in the AF CuO<sub>2</sub> planes causing a dynamic magnetic perturbation at the Gd site.

The static AF domain structure depends on external magnetic fields. In low magnetic fields the crystals have equal amounts of magnetic domains with  $M_s$  along one of the two

easy axes (that may be collateral or diagonal depending on the doping and the temperature). Magnetic fields rotate the sublattice magnetization, and in fields above a few teslas the crystals are magnetically single domain. A twofold and a larger fourfold anisotropic pinning is required to describe the wiping out of the domain structure by magnetic fields. In the diagonal phase an inhomogeneous hole distribution with an approximately squarelike (egg-box type) network of phase-separated regions is the likely source of the fourfold anisotropic part of the pinning. In the collateral phase a direct coupling of the spins to the lattice (i.e., magnetostriction) may also play a role.

No in-plane conductivity anisotropy was found in the frequency range of 10–90  $\text{cm}^{-1}$ . The most likely explanation for this negative result is that the magnetic field rotates the spins but leaves the underlying hole distribution unchanged. This view is contrary to the interpretation of the magnetoresistance in lightly doped YBCO and LaSCO by Ando *et al.*<sup>20,25</sup> In these works it was assumed that the magnetic field aligns the underlying array of linear stripes, rendering the sample electrically anisotropic.

Finally, we comment on the implication of our work to the polarization dependent Raman scattering results of Hackl *et al.*,<sup>30</sup> which are the most convincing demonstrations of an electrical excitation of phase-separated holes. Their interpretation holds both for diagonal stripes or a squarelike, egg-box-hole structure. Similarly to the IR transmission, no magnetic field dependence of the Raman scattering is expected for an egg-box like hole structure. The low-frequency fluctuations of AF domains at higher temperatures reflect weaker pinning and a gradual disappearance of the underlying hole-segregated regions, in accord with the broadening of the anomalous Raman peak. It is to be seen whether the rotation of the easy axis from diagonal to collateral as the temperature is increased in the Ca0.8% sample has a counterpart in the Raman spectra.

#### ACKNOWLEDGMENTS

This work was supported by the Hungarian state grants OTKA 60984 and TS 049881 and OTKA-DFG. A.J. is indebted to B. Horovitz (Ben-Gurion University of Negev, Israel) for illuminating discussions on the role of magnetostriction, and to R. Hackl and L. Tassini for discussions of their Raman spectroscopy results. We are indebted to G. Mihály (BUTE, Budapest) for dc resistivity experiments. T.F. was partially supported by the NCCR “MaNEP” of the Swiss National Science Fund and the Hungarian state grant OTKA PF 63954. L.M. was supported by the Szent-Györgyi program of the Hungarian Ministry of Education. We are indebted to G. L. Carr for developing the IR facilities at U12IR and to K. Holczer for continued discussions and support. Use of the National Synchrotron Light Source, Brookhaven National Laboratory, was supported by the U.S. Department of Energy, Office of Science, Office of Basic Energy Sciences, under Contract No. DE-AC02-98CH10886.

#### APPENDIX: THE ESR SPECTRUM OF $\text{Gd}^{3+}$ DOPED IN YBCO

The magnetic fine structure of the nearly spin-only  $J_{\text{Gd}} = 7/2$  angular momentum  $\text{Gd}^{3+}$  ion at the rare earth site of

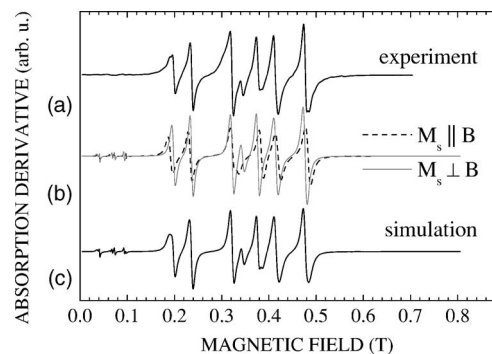


FIG. 12.  $\text{Gd}^{3+}$  ESR spectrum and simulation of the Ca2% YBCO sample at 20 K and 9 GHz for  $B \parallel [110]$ . (a) Measured spectrum. (b) Simulated spectra for the two types of orthogonal domains. The effective spin Hamiltonian parameters are  $b_2^0 = -1265$  MHz,  $b_4^0 = -192$  MHz,  $b_4^4 = 817$  MHz,  $b_4^2 = b_6^m = 0$ , and  $b_2^2 = 48$  MHz. Solid curve,  $M_s \perp B$ :  $g_{\perp} = 1.9882$  and  $O_2'^2$  is  $O_2^2$  rotated by  $3\pi/4$  around  $[001]$ , and linewidths 81 G from peak to peak. Dashed curve,  $M_s \parallel B$ :  $g_{\parallel} = 1.9924$  and  $O_2'^2$  is  $O_2^2$  rotated by  $\pi/4$  around  $[001]$ , and line widths 104 G from peak to peak. (c) Simulated spectrum with a 4:7 ratio of  $M_s \parallel B$  and  $M_s \perp B$  domains.

YBCO is well described by the effective spin Hamiltonian

$$H_{fs} = \sum_{m,n} c_n b_n^m O_n^m, \quad (\text{A1})$$

where  $n=2, 4$ , or  $6$ ;  $0 \leq m \leq n$  even;  $O_n^m$  are the Stevens operators;  $c_2=1/3$ ,  $c_4=1/60$ ,  $c_6=1/1260$ ; and  $b_n^m$  are the zero field splitting (ZFS) parameters.

The phenomenological ZFS parameters can be determined from the ESR spectra with high precision since the fine structure lines are narrow. Hence, they reflect small changes in the crystal fields sensitively. Figure 12 shows a spectrum whose most dominant features are the seven allowed fine structure transitions. In addition to tetragonal terms in Eq. (A1), i.e., those corresponding to  $m=0$  and 4, that follow from the crystal structure, the following term is required to describe the observed ESR spectra for fields in the  $\text{CuO}_2$  plane:

$$H_{fso} = \frac{1}{3} b_2^2 O_2'^2. \quad (\text{A2})$$

Here  $O_2'^2$  corresponds to the  $O_2^2$  Stevens operator but it is not fixed to the lattice; rather, it rotates with the antiferromagnetic sublattice magnetization,  $M_s$ . A possible reason for this could be magnetostriction that slightly distorts the tetragonal symmetry, and, e.g., if  $M_s \parallel [100]$ , the lattice constants parallel and perpendicular to  $M_s$  differ somewhat. However, contrary to our earlier view,<sup>24</sup> the data in hole-doped samples show that magnetostriction cannot be the main origin of the orthorhombic terms. For sample Ca0.8% as the temperature rises, the antiferromagnetic easy axis rotates from  $[110]$  to  $[100]$ , but the magnitude of  $b_2^2$  derived from the splitting of the fine structure remains the same. This rules out magnetostriction, which is expected to be much smaller for  $M_s$  along the  $[110]$  than the  $[100]$  direction. To solve the dilemma, we suggest that a term formally described by an orthorhombic

fine structure parameter arises from the magnetic interaction between  $Gd^{3+}$  and the  $CuO_2$  lattice. In this case the magnitude of  $b_2^2$  is proportional to the susceptibility anisotropy  $\chi$  of the  $CuO_2$  antiferromagnet, which is unaffected by the direction of the easy axis of  $M_s$ .

We describe the magnetic coupling of the  $Gd^{3+}$  ESR probe to the  $CuO_2$  lattice by an effective exchange Hamiltonian,

$$H_M = \sum J_1 S_{Gd} S_{Cu}, \quad (A3)$$

where  $J_1$  stands for an indirect coupling of  $Gd^{3+}$  to the antiferromagnetic magnetization of YBCO and the summation is over the eight first-neighbors.  $Gd^{3+}$  is directly coupled to the polarization of neighboring O atoms, which itself is coupled to the polarization of two neighboring Cu atoms. The rare earth ion is in a highly symmetric position within the antiferromagnetic  $CuO_2$  sandwich, and  $H_M$  does not shift the energies in first order of  $J_1$  in the absence of an external magnetic field. In a magnetic field perpendicular to  $M_s$ , the mean field ESR Knight shift of the fine structure lines is

$$\Delta B_K = -{}^{Gd}A\chi B, \quad (A4)$$

where  $\chi$  is the molar susceptibility tensor and  ${}^{Gd}A = zJ_1/(2Ng_{Gd}g_{Cu}\mu_B^2)$ . Here  $z=8$  is the number of Cu neighbors of Gd and  $N$  is the Avogadro number. For simplicity we take  $\chi_{||}=0$  and  $\chi=\chi_{\perp}$ . The  $Gd^{3+}$  ESR Knight shift is important at high magnetic fields, and is proportional to the  ${}^{89}Y$  NMR Knight shift for doped YBCO in a broad doping concentration range.<sup>36</sup>

There is a further non-negligible term, second order in  $J_1$ , that arises from the polarization of neighboring Cu (and O)

atoms by the  $Gd^{3+}$  spins. In a mean-field treatment, neglecting terms that are isotropic in the  $CuO_2$  plane,

$$H_{M2} = \frac{1}{3}b_2^2 O_2'^2, \quad (A5a)$$

with

$$b_2^2 = \frac{3}{2} \frac{zJ_1^2 \chi_1}{2N(g_{Cu}\mu_B)^2 \hbar}, \quad (A5b)$$

where  $\chi_1$  describes the polarizability of the Cu spins by the  $Gd^{3+}$  exchange field perpendicular to  $M_s$ , and  $O_2'^2$  is the  $O_2^2$  Stevens operator rotated the same way as what is needed to turn the  $[100]$  vector parallel to  $M_s$ . In a single fluid model  $\chi_1$  is comparable to  $\chi$ , the anisotropy of the macroscopic susceptibility. The magnetic interaction changes the spectrum formally the same way as an orthorhombic distortion of the crystal.

The measured values are  ${}^{Gd}A=1.5 \text{ T}^2 \text{ mol/J}$ ,<sup>36</sup>  $b_2^2=48 \text{ MHz}$  and  $\chi=1.4 \times 10^{-3} \text{ J/T}^2 \text{ mol}$ ,<sup>25</sup> so that we deduce  $\chi_1=0.13\chi$  for the polarizability of the  $CuO_2$  plane by the  $Gd^{3+}$  ions. In a single fluid model  $\chi_1$  would be equal to  $\sum_q \chi_q \cos(a_0 q_x/2) \cos(a_0 q_y/2)$ , i.e., the nonlocal response of the  $CuO_2$  plane weighted by the form factor corresponding to the eight Cu nearest neighbors of the  $Gd^{3+}$ . This should be roughly the same as  $\chi$ . Clearly, a more sophisticated model of the coupling of  $Gd^{3+}$  to  $CuO_2$  planes would be necessary for a quantitative description. However, it reproduces the main features: the main axes rotate with the magnetization but the magnitude of the shifts of the fine structure lines remains the same.

\*Corresponding author. Electronic address: atj@szfki.hu

<sup>1</sup>J. Zaanen and O. Gunnarsson, Phys. Rev. B **40**, 7391 (1989).

<sup>2</sup>H. J. Schulz, Phys. Rev. Lett. **64**, 1445 (1990).

<sup>3</sup>K. Machida, Physica C **158**, 192 (1989).

<sup>4</sup>M. Kato, K. Machida, H. Nakanishi, and M. Fujita, J. Phys. Soc. Jpn. **59**, 1047 (1990).

<sup>5</sup>V. J. Emery, S. A. Kivelson, and H. Q. Lin, Phys. Rev. Lett. **64**, 475 (1990).

<sup>6</sup>A. H. Castro Neto and C. Morais Smith, in *Strong Interactions in Low Dimensions*, edited by D. Baeriswyl and L. Degiorgi (Kluwer, Dordrecht, 2004), Vol. 25, Chap. 9, p. 277.

<sup>7</sup>G. Seibold, F. Becca, F. Bucci, C. Castellani, C. Di Castro, and M. Grilli, Eur. Phys. J. B **13**, 87 (2000).

<sup>8</sup>B. V. Fine, Phys. Rev. B **70**, 224508 (2004).

<sup>9</sup>B. Horowitz, Phys. Rev. B **69**, 140501(R) (2004).

<sup>10</sup>B. I. Shraiman and E. D. Siggia, Phys. Rev. Lett. **62**, 1564 (1989).

<sup>11</sup>J. M. Tranquada, D. J. Buttrey, V. Sachan, and J. E. Lorenzo, Phys. Rev. Lett. **73**, 1003 (1994).

<sup>12</sup>Ch. Niedermayer, C. Bernhard, T. Blasius, A. Golnik, A. Moodenbaugh, and J. I. Budnick, Phys. Rev. Lett. **80**, 3843 (1998).

<sup>13</sup>S.-W. Cheong, G. Aeppli, T. E. Mason, H. Mook, S. M. Hayden, P. C. Canfield, Z. Fisk, K. N. Clausen, and J. L. Martinez, Phys.

Rev. Lett. **67**, 1791 (1991).

<sup>14</sup>T. E. Mason, G. Aeppli, and H. A. Mook, Phys. Rev. Lett. **68**, 1414 (1992).

<sup>15</sup>S. Wakimoto, G. Shirane, Y. Endoh, K. Hirota, S. Ueki, K. Yamada, R. J. Birgeneau, M. A. Kastner, Y. S. Lee, P. M. Gehring, and S. H. Lee, Phys. Rev. B **60**, R769 (1999).

<sup>16</sup>M. Matsuda, M. Fujita, K. Yamada, R. J. Birgeneau, M. A. Kastner, H. Hiraka, Y. Endoh, S. Wakimoto, and G. Shirane, Phys. Rev. B **62**, 9148 (2000).

<sup>17</sup>S. Wakimoto, R. J. Birgeneau, M. A. Kastner, Y. S. Lee, R. Erwin, P. M. Gehring, S. H. Lee, M. Fujita, K. Yamada, Y. Endoh, K. Hirota, and G. Shirane, Phys. Rev. B **61**, 3699 (2000).

<sup>18</sup>H. A. Mook, P. C. Dai, F. Dogan, and R. D. Hunt, Nature (London) **404**, 729 (2000).

<sup>19</sup>V. Hinkov, S. Pailhes, P. Bourges, Y. Sidis, A. Ivanov, A. Kulkov, C. T. Lin, D. P. Chen, C. Bernhard, and B. Keimer, Nature (London) **430**, 650 (2004).

<sup>20</sup>Y. Ando, A. N. Lavrov, and K. Segawa, Phys. Rev. Lett. **83**, 2813 (1999).

<sup>21</sup>A. Jánossy, F. Simon, and T. Fehér, Phys. Rev. Lett. **85**, 474 (2000).

<sup>22</sup>E. Cimpoiasu, V. Sandu, C. C. Almasan, A. P. Paulikas, and B. W. Veal, Phys. Rev. B **65**, 144505 (2002).

- <sup>23</sup>P. Burllet, J. Y. Henry, and L. P. Regnault, *Physica C* **296**, 205 (1998).
- <sup>24</sup>A. Jánossy, F. Simon, T. Fehér, A. Rockenbauer, L. Korecz, C. Chen, A. J. S. Chowdhury, and J. W. Hodby, *Phys. Rev. B* **59**, 1176 (1999).
- <sup>25</sup>Y. Ando, A. N. Lavrov, and S. Komiya, *Phys. Rev. Lett.* **90**, 247003 (2003).
- <sup>26</sup>S. Ono, S. Komiya, A. N. Lavrov, Y. Ando, F. F. Balakirev, J. B. Betts, and G. S. Boebinger, *Phys. Rev. B* **70**, 184527 (2004).
- <sup>27</sup>M. Dumm, S. Komiya, Y. Ando, and D. N. Basov, *Phys. Rev. Lett.* **91**, 077004 (2003).
- <sup>28</sup>F. Venturini, Q.-M. Zhang, R. Hackl, A. Lucarelli, S. Lupi, M. Ortolani, P. Calvani, N. Kikugawa, and T. Fujita, *Phys. Rev. B* **66**, 060502(R) (2002).
- <sup>29</sup>L. Tassini, F. Venturini, Q.-M. Zhang, R. Hackl, N. Kikugawa, and T. Fujita, *Phys. Rev. Lett.* **95**, 117002 (2005).
- <sup>30</sup>R. Hackl, L. Tassini, F. Venturini, A. Erb, C. Hartinger, N. Kikugawa, and T. Fujita, *J. Phys. Chem. Solids* **67**, 289 (2006).
- <sup>31</sup>A. Erb, E. Walker, and R. Flukiger, *Physica C* **258**, 9 (1996).
- <sup>32</sup>A. Jánossy, T. Fehér, and A. Erb, *Phys. Rev. Lett.* **91**, 177001 (2003).
- <sup>33</sup>M. T. Causa, C. Fainstein, G. Nieva, R. Sanchez, L. B. Steren, M. Tovar, R. Zysler, D. C. Vier, S. Schultz, S. B. Oseroff, Z. Fisk, and J. L. Smith, *Phys. Rev. B* **38**, 257 (1988).
- <sup>34</sup>C. Rettori, D. Rao, S. Oseroff, R. D. Zysler, M. Tovar, Z. Fisk, S.-W. Cheong, S. Schultz, and D. C. Vier, *Phys. Rev. B* **44**, 826 (1991).
- <sup>35</sup>A. Rockenbauer, A. Jánossy, L. Korecz, and S. Pekker, *J. Magn. Reson.* **97**, 540 (1992).
- <sup>36</sup>A. Jánossy, L.-C. Brunel, and J. R. Cooper, *Phys. Rev. B* **54**, 10186 (1996).
- <sup>37</sup>L. Mihály, D. Talbayev, L. F. Kiss, J. Zhou, T. Fehér, and A. Jánossy, *Phys. Rev. B* **69**, 024414 (2004).
- <sup>38</sup>K. Machida and M. Ichioka, *J. Phys. Soc. Jpn.* **68**, 2168 (1999).